

Interface induced spin-orbit interaction in silicon quantum dots and prospects for scalability

Rifat Ferdous,¹ Kok W. Chan,² Menno Veldhorst,³ J.C.C. Hwang,² C. H. Yang,²
Gerhard Klimeck,¹ Andrea Morello,² Andrew S. Dzurak,² and Rajib Rahman¹

¹*Network for Computational Nanotechnology, Purdue University, West Lafayette, IN 47907, USA*

²*Centre for Quantum Computation and Communication Technology,
School of Electrical Engineering and Telecommunications,*

The University of New South Wales, Sydney, New South Wales 2052, Australia

³*QuTech and Kavli Institute of Nanoscience, TU Delft, Lorentzweg 1, 2628CJ Delft, the Netherlands*

(Dated: August 3, 2017)

We identify the presence of monoatomic steps at the Si/SiGe or Si/SiO₂ interface as a dominant source of variations in the dephasing time of Si quantum dot (QD) spin qubits. First, using atomistic tight-binding calculations we show that the g -factors and their Stark shifts undergo variations due to these steps. We compare our theoretical predictions with experiments on QDs at a Si/SiO₂ interface, in which we observe significant differences in Stark shifts between QDs in two different samples. We also experimentally observe variations in the g -factors of one-electron and three-electron spin qubits realized in three neighboring QDs on the same sample, at a level consistent with our calculations. The dephasing times of these qubits also vary, most likely due to their varying sensitivity to charge noise, resulting from different interface conditions. More importantly, from our calculations we show that by employing the anisotropic nature of the spin-orbit interaction (SOI) in a Si QD, we can minimize and control these variations. Ultimately, we predict that the dephasing times of the Si QD spin qubits will be anisotropic and can be improved by at least an order of magnitude, by aligning the external DC magnetic field towards specific crystal directions.

A scalable quantum computing architecture requires reproducibility and control over key qubit properties, such as resonance frequency, coherence time, etc. Variability in such parameters among qubits of a large-scale quantum computer would necessitate individual qubit characterization and control[1], while excessive variability could even make scaling impractical. In case of significant variability in the dephasing time, the performance of a large-scale quantum computer might be limited by the fidelity of the qubit that decoheres the fastest.

Spin qubits hosted in silicon (Si) quantum dots (QD)[2] have been showing promise as a potential building block for a large-scale quantum computer[3], because of their compatibility with already existing CMOS technology and the long coherence times available due to the presence of negligible nuclear spins in isotopically purified ²⁸Si[4]. Single[5–10] and two qubit[11] gates have been demonstrated already. To move forward with increasing numbers of qubits[1, 12–14], we have to study possible sources that can cause variations in the coherence time and limit the performance of these qubits.

In this letter, we provide a microscopic understanding of the dephasing time T_2^* of Si QD spin qubits. We show that electrical noise modulates the electron g -factor through spin-orbit interaction (SOI) and causes dephasing. Moreover, the atomic scale details of the interface controls the sensitivity of the g -factor to the electric field or noise and hence introduce variability in the T_2^* times. We experimentally observe variations in the g -factors, their gate voltage dependence and T_2^* times among spin qubits hosted in gate-defined quantum dots formed at a Si/SiO₂ interface. Finally we predict that, due to the anisotropic nature of the SOI in Si QDs, the T_2^* times

will be anisotropic and hence can be improved and their variability can be reduced as well by choosing the appropriate direction of the external magnetic field.

The energy levels of interest in a Si QD for qubit operations are two low lying conduction band valley states v_- and v_+ , each split in two spin levels in the presence of a DC magnetic field, B_{ext} . Until recently, the main focus has been to increase the valley splitting energy to create well isolated states. In metal-oxide-semiconductor based Si QDs, this is now routinely achieved[8, 15]. However, it turns out that the spin splitting ($E_{ZS}^{\pm} = g_{\pm}\mu_B B_{\text{ext}}$, where μ_B is the Bohr magneton) and also the dephasing time T_2^* are valley dependent[9, 16–19] and, as we will show experimentally, is sample-to-sample dependent.

In a Si quantum well or dot, the presence of structure inversion asymmetry (SIA) introduces the Rashba SOI[20–22]. Though it is known that due to the lack of bulk inversion asymmetry (BIA), the Dresselhaus SOI is absent from bulk Si, interface inversion asymmetry (IIA) contributes a Dresselhaus-like term in interface confined structures in Si[20–22]. Both the Rashba and Dresselhaus SOI modify the electron g -factors in a Si QD, and enable the Stark shift of the g -factors through gate voltage tuning[8, 15, 16]. The different sign of the Rashba (α_{\pm}) and Dresselhaus coefficients (β_{\pm}) results in different g -factors among the two valley states[16]. The Dresselhaus contribution is usually much stronger than the Rashba SOI[19, 22], and dominates the g -factor renormalization [19]. These SOI effects also make the qubits susceptible to electrical noise.

In a Si QD with a strong vertical electric field, the electrons are usually confined to only one interface. A monoatomic shift in the location of this interface re-

sults in a sign inversion of the Dresselhaus coefficient (β), while the Rashba coefficient (α) remains unchanged[20–22]. In practice, Si/SiGe or Si/SiO₂ interfaces certainly contain roughness, i.e monoatomic steps[23–25]. A non-ideal interface with monoatomic steps can be thought of as multiple smooth interface regions, where interfaces of neighboring regions are shifted by one atomic layer with respect to each other. Thus the neighboring regions will have opposite signs of β . An electron wavefunction spread over multiple such regions will witness multiple local β s and the effective β will be a weighted average. Thus the presence of interface steps can change both the sign and magnitude of the effective Dresselhaus contribution to the electron g -factors in a Si QD[19]. To accurately understand these atomic-scale physics of the interface, here we use spin resolved $sp^3d^5s^*$ tight-binding model, where the effects of the SOI comes out automatically based on the atomic arrangement of the QD, without any pre-assumption about the Rashba or Dresselhaus SOI.

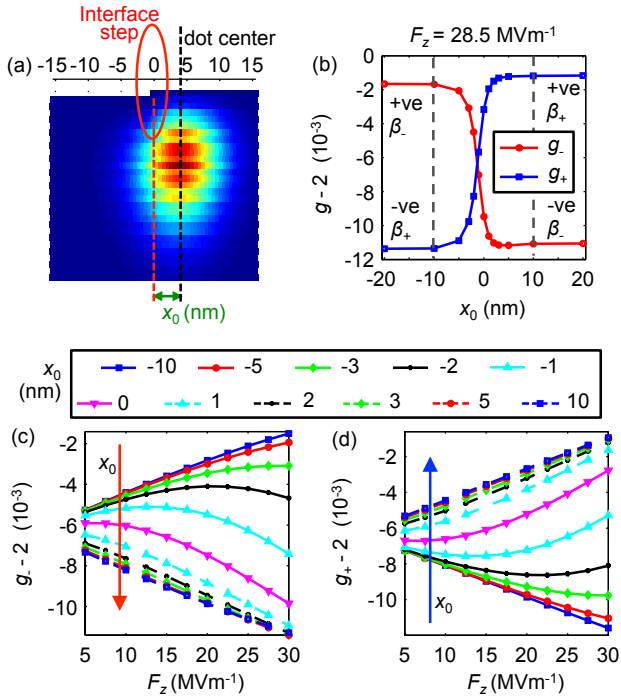


FIG. 1. Effect of interface steps on g -factors and their Stark shifts in a Si QD from atomistic tight-binding calculation. (a) An electron wavefunction subject to an interface step. (b) Variation in the g -factors for both valley states (g_- and g_+), as a function of x_0 for vertical electric field $F_z = 28.5 \text{ MVm}^{-1}$ [15]. F_z dependence of (c) g_- and (d) g_+ for various x_0 .

Fig. 1 shows how a monoatomic step at the interface of a Si QD can affect the g -factors of the valley states and their electric field dependence, with an external magnetic field along the [110] crystal orientation, from atomistic tight-binding simulations. An electron wavefunction near

an interface step is shown in Fig. 1a. The distance between the dot center and the location of the edge of the interface step is denoted by x_0 . The dot radius is around 10 nm. So for $x_0 < -10 \text{ nm}$ the dot is completely on the left side of the step and has different g -factors ($g_- > g_+$) compared to that ($g_+ > g_-$) for $x_0 > 10 \text{ nm}$, when the dot is completely on the right side of the step, as seen in Fig. 1b. For $-10 \text{ nm} < x_0 < 10 \text{ nm}$, the g -factors are a weighted average of those of the two sides based on the dot location. To understand this atomistic calculation we use an analytic effective mass model that relates g_{\pm} in a Si QD, with the Rashba and Dresselhaus SOI[16, 19]. We briefly summarize this model in the Supplemental Material[26]. For B_{ext} along the [110] crystal orientation

$$\delta g_{\pm}^{[110]} = 2 \frac{|e| \langle z \rangle}{\mu_B \hbar} (-\alpha_{\pm} + \beta_{\pm}) \quad (1)$$

Here, $|e|$ is the electron charge, $\langle z \rangle$ is the spread of the electron wavefunction along the vertical direction z ([001]) and \hbar is the reduced Planck constant. Now, in a Si QD, $\beta \gg \alpha$ [19, 22], and so

$$\delta g_{\pm}^{[110]} \approx 2 \frac{|e| \langle z \rangle}{\mu_B \hbar} \beta_{\pm} \quad (2)$$

As previously discussed, β has a different sign between the two sides of the step. When the location of the dot changes with respect to the step, the weighted average of the positive and negative β s change, which changes the g -factors.

Figs. 1c and 1d show that the Stark shift of the g -factors, as a function of the confining vertical electric field F_z , for both valley states are also affected by the presence of an interface step. The differential change in the g -factors with electric field, $\frac{dg_{\pm}}{dF_z}$, can vary in both sign and magnitude depending on the location of the step with respect to the dot center. This behavior can also be explained by equation 2, with the change in β near an interface step. For example in Fig. 1c, for $x_0 \approx -10 \text{ nm}$, the dot is completely on the left side of the step, where the v_- valley state has positive β . Thus an increase in β_- with increasing F_z increases g_- as well, hence a positive $\frac{dg_-}{dF_z}$. On the other hand, when the dot is completely on the right side of the step, at $x_0 \approx 10 \text{ nm}$, β_- is negative. Thus increasing F_z increases $|\beta_-|$ but decreases g_- and thus results in a negative $\frac{dg_-}{dF_z}$. For $-10 \text{ nm} < x_0 < 10 \text{ nm}$, $\frac{dg_-}{dF_z}$ changes gradually with x_0 . We see a similar but opposite change for g_+ in Fig. 1d.

Similar variations in the g -factors, and their gate voltage dependence, are measured in gate-defined quantum dots formed at a Si/SiO₂ interface for two different samples (A and B) with similar architecture. In sample A we operated spin qubits in three neighboring QDs while in sample B we studied a qubit in a single QD. In Fig. 2a, we show a schematic diagram of one of the devices (sample A) measured experimentally. In sample A, we observe variations in one-electron and three-electron g -factors among three neighboring QDs (Q_1, Q_2, Q_3), as

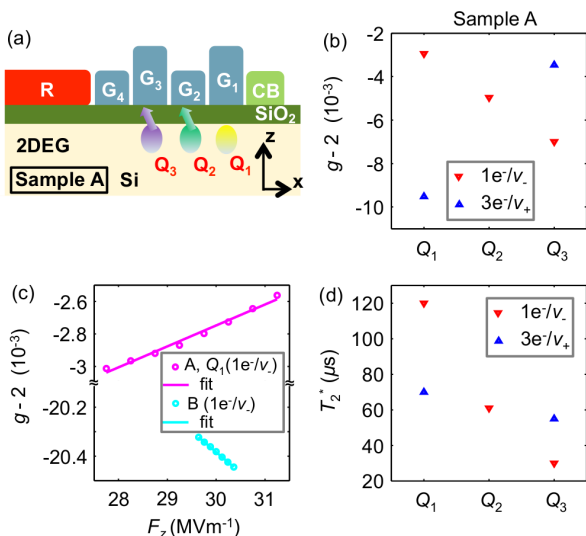


FIG. 2. Schematic diagram of the experimental sample and observed dot-to-dot variations. (a) Cross sectional schematic of sample A. CB acts as a lateral confinement gate in the formation of quantum dots under gates G_1 , G_2 , and G_3 . G_4 is used as a tunnel barrier for loading/unloading of electrons from the 2DEG formed under the reservoir (R) gate. (b) Variation in the g -factors, both one-electron (g_-) and three-electron (g_+), among three neighboring quantum dots (Q_1 , Q_2 , Q_3) formed at the Si/SiO₂ interface in sample A. (c) One-electron Stark shift of Q_1 from sample A and one QD from sample B plotted together as a function of the vertical electric field, F_z . Note that both samples were measured in different dilution fridges and there is an unknown B_{ext} offset in sample B, contributing to larger discrepancy in its g -factor from 2. (d) Observed variations in the dephasing times among qubits in sample A.

shown in Fig. 2b. We understand that the one-electron (three-electron) qubit corresponds to an electron occupying the lower (higher) energy valley state v_- (v_+)[16]. We could not achieve three-electron spin resonance for Q_2 as it was strongly coupled to the other dots. Fig. 2c shows the Stark shift of Q_1 on sample A and one QD on another sample B. We see here that the g_- of Q_1 has opposite dependence on F_z compared to that of the QD in sample B. These observed variations in both the Stark shifts and the g -factors qualitatively agree with the theoretically predicted variations shown in Fig. 1. We therefore conclude that these experimentally observed variations are primarily due to different interface conditions associated with each of the QDs.

We also observe variations in the measured T_2^* times for both valley states of the three QDs, as shown in Fig. 2d. The T_2^* times were extracted by performing Ramsey experiments on all of the qubits in sample A, as shown in the Supplemental Material[26].

The observed variations in T_2^* can be explained from the measured (Fig. 2c) and predicted (Fig. 1c,d) variations in $|dg_{\pm}/dF_z|$ with interface steps. The larger the $|dg_{\pm}/dF_z|$,

the more sensitive the qubit is to electrical noise. The dephasing time due to nuclear spin fluctuations is given in refs. [27, 28] and in our samples, which employ an isotopically enriched ²⁸Si substrate, these times are very long. In the absence of nuclear spin, we can relate T_2^* times with electrical noise in a similar way,

$$T_2^* = \frac{\sqrt{2}\hbar}{\Delta F_z |dg_{\pm}/dF_z| \mu_B B_{\text{ext}}} \quad (3)$$

Here, ΔF_z is the standard deviation of the electric field fluctuation seen by the dot, due to electrical noise on the gate. For Q_1 in sample A, we extract $|dg_-/dF_z| \approx 1.1 \times 10^{-10}$ mV⁻¹ from Fig. 2c and estimate $\Delta F_z \approx 870$ Vm⁻¹ for $T_2^* = 120$ μ s. When we compare the T_2^* times between the two valley states of Q_1 , we see $T_2^*(v_-, Q_1) \approx 1.7 T_2^*(v_+, Q_1)$ and from ref. [16] we find, $|dg_+/dF_z| \approx 2.2 |dg_-/dF_z|$. This comparison also shows how $1/T_2^*$ almost linearly depends on $|dg_{\pm}/dF_z|$ as predicted by equation 3. Thus variations in $|dg_{\pm}/dF_z|$ due to different interface conditions among different qubits will result in a variability in the dephasing time.

The calculations of Fig. 1 and the experimental observations of Fig. 2 highlight the device-to-device variability issues that would require individual knowledge of each qubit, and impose a challenge to the implementation of a large scale quantum computer. Any possible way of reducing the variability is crucial to the scale up of Si QD spin qubits. Also an increase in T_2^* , regardless of the interface condition, will aid scalability. Next we investigate ways to improve these issues.

One obvious way to suppress these variabilities and gain more control over the g -factors, their tunability and the dephasing times, is to minimize interface roughness, which is a well known fabrication challenge. Here we propose an alternate approach. As predicted in ref. [19], the g -factors in a Si QD are anisotropic. We can study the anisotropy from a simplified expression[19, 26],

$$\delta g_{\pm} \approx 2 \frac{|e| \langle z \rangle}{\mu_B \hbar} (-\alpha_{\pm} + \beta_{\pm} \sin 2\phi) \quad (4)$$

Here, ϕ is the angle of the external magnetic field with the [100] crystal orientation. From equation 4 we see that the contribution of the Dresselhaus SOI is anisotropic. Thus by changing the direction of B_{ext} we can tune the Dresselhaus contribution. For $\phi = 0^\circ/90^\circ/180^\circ/270^\circ$, the Dresselhaus contribution will be negligible. For example, when B_{ext} is along [100], $\phi = 0^\circ$ and

$$\delta g_{\pm}^{[100]} \approx -2 \frac{|e| \langle z \rangle}{\mu_B \hbar} \alpha_{\pm} \quad (5)$$

Comparing equation 2 and 5 we see that,

$$\frac{\delta g_{\pm}^{[100]}}{\delta g_{\pm}^{[110]}} \approx \frac{\alpha_{\pm}}{\beta_{\pm}} \quad (6)$$

As the effect of the monoatomic steps are more dramatic on β_{\pm} , the change in g_{\pm} and $\frac{dg_{\pm}}{dF_z}$ with interface steps should be smaller for B_{ext} along [100] compared to that for [110]. Moreover, since $\beta_{\pm} \gg \alpha_{\pm}$ [19, 22], $\frac{dg_{\pm}}{dF_z}$ itself will be much smaller for [100].

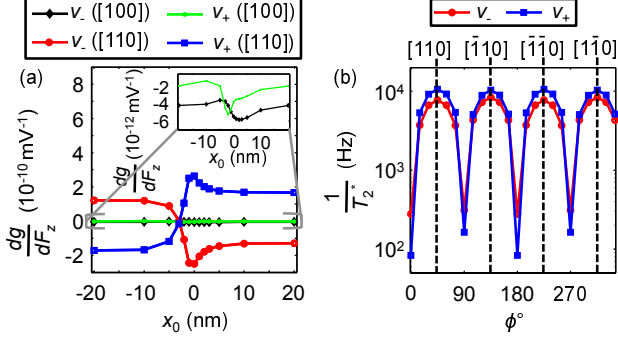


FIG. 3. (a) Change in $\frac{dg_{\pm}}{dF_z}$ as a function of x_0 with B_{ext} along [110] and [100] (inset), for $F_z = 28.5 \text{ MVm}^{-1}$, calculated using atomistic tight-binding model. (b) $\frac{1}{T_2}$ with respect to the direction of B_{ext} , ϕ for $x_0 = 6$ nm, $F_z = 28.5 \text{ MVm}^{-1}$ and $B_{\text{ext}} = 1.4015$ T.

Fig. 3a shows variations in $\frac{dg_{\pm}}{dF_z}$ with x_0 for B_{ext} along [110] and [100]. Though there are variations in $\frac{dg_{\pm}}{dF_z}$ with x_0 for B_{ext} along [100], as shown by the inset of Fig. 3a, these variations and also $\frac{dg_{\pm}}{dF_z}$ themselves are negligible, when compared to that along [110]. Variation of g_{\pm} with x_0 , will also be negligible for B_{ext} along [100], as shown in the Supplemental Material[26]. Such phenomena will have a critical impact on the realization of a large scale quantum computer made of Si QDs. If the external magnetic field is along the [100] crystal orientation, all the qubits will have negligible variations in g_{\pm} , $\frac{dg_{\pm}}{dF_z}$, and consequently in T_2^* even in the presence of varying interface conditions. Very small $|\frac{dg_{\pm}}{dF_z}|$ along [100] would also result in very long T_2^* times. From Fig. 3a, we calculate the average $|\frac{dg_{\pm}}{dF_z}|$ over different values of x_0 and find that, $\text{avg}\left(\left|\frac{dg_{-}}{dF_z}([110])\right|\right) \approx 30 \text{ avg}\left(\left|\frac{dg_{-}}{dF_z}([100])\right|\right)$ and $\text{avg}\left(\left|\frac{dg_{+}}{dF_z}([110])\right|\right) \approx 50 \text{ avg}\left(\left|\frac{dg_{+}}{dF_z}([100])\right|\right)$. If a linear relationship between $\frac{1}{T_2}$ and $|\frac{dg_{\pm}}{dF_z}|$ holds, as predicted by equation 3, the T_2^* times can be longer than 1 ms, provided that other noise sources do not contribute significantly.

In Fig. 3b, the angular dependence of $\frac{1}{T_2}$ for $x_0 = 6$ nm, is shown. From atomistic simulations we calculated $\frac{dg_{\pm}}{dF_z}$

for different ϕ and used equation 3 to calculate $\frac{1}{T_2^*}$ for $\Delta F_z \approx 870 \text{ Vm}^{-1}$ and $B_{\text{ext}} = 1.4$ T. The anisotropy in Fig. 3b can be understood by connecting equation 3 and 4,

$$\frac{1}{T_2^*(v_{\pm})} = \Delta F_z \frac{2|e|B_{\text{ext}}}{\sqrt{2}\hbar^2} \left| -\frac{d(\langle z \rangle \alpha_{\pm})}{dF_z} + \sin 2\phi \frac{d(\langle z \rangle \beta_{\pm})}{dF_z} \right| \quad (7)$$

As $\frac{d(\langle z \rangle \beta_{\pm})}{dF_z} \gg \frac{d(\langle z \rangle \alpha_{\pm})}{dF_z}$ a large increase in T_2^* is achievable by orientating B_{ext} along [100]/[010]/ $[\bar{1}00]$ /[0 $\bar{1}0$].

Now, a decrease in $|\frac{dg_{\pm}}{dF_z}|$ would also mean a reduced tunability of the g -factors, which is necessary for selective addressing of individual qubits. However, an increase in T_2^* times will result in a narrower electron spin resonance (ESR) linewidth, $\delta f_{\text{FWHM}} = \frac{2\sqrt{\ln 2}}{\pi T_2^*}[9]$, which would then require a smaller difference in g -factors between qubits to individually address them. As the g -factors and $\frac{dg_{\pm}}{dF_z}$ have lesser variations with interface roughness along [100], the g -factor difference between qubits can be more controlled. Moreover, by tuning the direction of the external magnetic field a desired trade off between large $|\frac{dg_{\pm}}{dF_z}|$ and large T_2^* times can be achieved.

Orienting the magnetic field along the [100] crystal orientation results in a Dresselhaus SOI with only off-diagonal components [26]. Therefore, electric field fluctuations, to first order, contribute to spin dephasing through the weaker Rashba SOI, ensuring a long T_2^* time. At the same time, a resonant oscillating electric field can induce electric dipole spin resonance (EDSR) through the off-diagonal Dresselhaus coupling. Since T_2^* is long under these conditions, coherent operations can be expected even for relatively weak EDSR driving strength, and without invoking the use of micromagnets[9].

To conclude, we experimentally observe variations in the electron g -factors and their sensitivity to electric field, which also leads to variability in the dephasing times among Si/SiO₂ quantum dot spin qubits. We identify that the source of the variation is the presence of random monoatomic steps at the interface. To gain control over these key qubit parameters one has to minimize interface roughness, which is challenging to achieve. We show here that even in the presence of interface steps we can control and minimize these variations by taking advantage of the anisotropic SOI in a Si QD. Importantly, we can increase T_2^* times if we align the external magnetic field along the [100] crystal orientation, rather than along [110]. Pointing the external B-field along [100] will also help to reduce the SOI induced dephasing in Si QD devices with integrated micro-magnets, as SOI also contributes to the g -factors in these devices[19].

[1] L. M. K. Vandersypen, H. Bluhm, J. S. Clarke, A. S. Dzurak, R. Ishihara, A. Morello, D. J. Reilly, L. R. Schreiber,

and M. Veldhorst, (2016), arXiv:1612.05936.

- [2] D. Loss and D. P. DiVincenzo, *Phys. Rev. A* **57**, 120 (1998).
- [3] F. A. Zwanenburg, A. S. Dzurak, A. Morello, M. Y. Simmons, L. C. L. Hollenberg, G. Klimeck, S. Rogge, S. N. Coppersmith, and M. A. Eriksson, *Rev. Mod. Phys.* **85**, 961 (2013).
- [4] K. M. Itoh and H. Watanabe, *MRS Commun.* **4**, 143 (2014).
- [5] B. M. Maune, M. G. Borselli, B. Huang, T. D. Ladd, P. W. Deelman, K. S. Holabird, A. A. Kiselev, I. Alvarado-Rodriguez, R. S. Ross, A. E. Schmitz, M. Sokolich, C. A. Watson, M. F. Gyure, and A. T. Hunter, *Nature* **481**, 344 (2012).
- [6] D. Kim, Z. Shi, C. B. Simmons, D. R. Ward, J. R. Prance, T. S. Koh, J. K. Gamble, D. E. Savage, M. G. Lagally, M. Friesen, S. N. Coppersmith, and M. A. Eriksson, *Nature* **511**, 70 (2014).
- [7] X. Wu, D. R. Ward, J. R. Prance, D. Kim, J. K. Gamble, R. T. Mohr, Z. Shi, D. E. Savage, M. G. Lagally, M. Friesen, S. N. Coppersmith, and M. A. Eriksson, *Proc. Natl. Acad. Sci. U. S. A.* **111**, 11938 (2014).
- [8] M. Veldhorst, J. C. C. Hwang, C. H. Yang, A. W. Leenstra, B. de Ronde, J. P. Dehollain, J. T. Muhonen, F. E. Hudson, K. M. Itoh, A. Morello, and A. S. Dzurak, *Nat. Nanotechnol.* **9**, 981 (2014).
- [9] E. Kawakami, P. Scarlino, D. R. Ward, F. R. Braakman, D. E. Savage, M. G. Lagally, M. Friesen, S. N. Coppersmith, M. A. Eriksson, and L. M. K. Vandersypen, *Nat. Nanotechnol.* **9**, 666 (2014).
- [10] K. Eng, T. D. Ladd, A. Smith, M. G. Borselli, A. A. Kiselev, B. H. Fong, K. S. Holabird, T. M. Hazard, B. Huang, P. W. Deelman, I. Milosavljevic, A. E. Schmitz, R. S. Ross, M. F. Gyure, and A. T. Hunter, *Sci. Adv.* **1** (2015).
- [11] M. Veldhorst, C. H. Yang, J. C. C. Hwang, W. Huang, J. P. Dehollain, J. T. Muhonen, S. Simmons, A. Laucht, F. E. Hudson, K. M. Itoh, A. Morello, and A. S. Dzurak, *Nature* **526**, 410 (2015).
- [12] D. M. Zajac, T. M. Hazard, X. Mi, E. Nielsen, and J. R. Petta, *Phys. Rev. Appl.* **6**, 54013 (2016).
- [13] C. Jones, M. A. Fogarty, A. Morello, M. F. Gyure, A. S. Dzurak, and T. D. Ladd, (2016), arXiv:1608.06335.
- [14] M. Veldhorst, H. G. J. Eenink, C. H. Yang, and A. S. Dzurak, (2016), arXiv:1609.09700.
- [15] C. H. Yang, A. Rossi, R. Ruskov, N. S. Lai, F. A. Mohiyaddin, S. Lee, C. Tahan, G. Klimeck, A. Morello, and A. S. Dzurak, *Nat. Commun.* **4**, 2069 (2013).
- [16] M. Veldhorst, R. Ruskov, C. H. Yang, J. C. C. Hwang, F. E. Hudson, M. E. Flatté, C. Tahan, K. M. Itoh, A. Morello, and A. S. Dzurak, *Phys. Rev. B* **92**, 201401 (2015).
- [17] P. Scarlino, E. Kawakami, D. R. Ward, D. E. Savage, M. G. Lagally, M. Friesen, S. N. Coppersmith, M. A. Eriksson, and L. M. K. Vandersypen, *Phys. Rev. Lett.* **115**, 106802 (2015).
- [18] P. Scarlino, E. Kawakami, T. Jullien, D. R. Ward, D. E. Savage, M. G. Lagally, M. Friesen, S. N. Coppersmith, M. A. Eriksson, and L. M. K. Vandersypen, *Phys. Rev. B* **95**, 165429 (2017).
- [19] R. Ferdous, E. Kawakami, P. Scarlino, M. P. Nowak, D. R. Ward, D. E. Savage, M. G. Lagally, S. N. Coppersmith, M. Friesen, M. A. Eriksson, L. M. K. Vandersypen, and R. Rahman, (2017), arXiv:1702.06210.
- [20] L. E. Golub and E. L. Ivchenko, *Phys. Rev. B* **69**, 115333 (2004).
- [21] M. O. Nestoklon, L. E. Golub, and E. L. Ivchenko, *Phys. Rev. B* **73**, 235334 (2006).
- [22] M. O. Nestoklon, E. L. Ivchenko, J.-M. Jancu, and P. Voisin, *Phys. Rev. B* **77**, 155328 (2008).
- [23] H. J. W. Zandvliet and H. B. Elswijk, *Phys. Rev. B* **48**, 14269 (1993).
- [24] M. Friesen, M. A. Eriksson, and S. N. Coppersmith, *Appl. Phys. Lett.* **89**, 202106 (2006).
- [25] N. Kharche, M. Prada, T. B. Boykin, and G. Klimeck, *Appl. Phys. Lett.* **90**, 092109 (2007).
- [26] See Supplemental Material.
- [27] R. Hanson, L. P. Kouwenhoven, J. R. Petta, S. Tarucha, and L. M. K. Vandersypen, *Rev. Mod. Phys.* **79**, 1217 (2007).
- [28] I. A. Merkulov, A. L. Efros, and M. Rosen, *Phys. Rev. B* **65**, 205309 (2002).

ACKNOWLEDGMENT

This work was supported by the U.S. Army Research Office (W911NF-13-1-0024, W911NF-12-0607), the Australian Research Council (CE11E0001017), and the NSW Node of Australian National Fabrication Facility. Computational resources on nanoHUB.org, funded by the NSF grant EEC-0228390, were used.

Supplementary Materials for ‘Interface induced spin-orbit interaction in silicon quantum dots and prospects for scalability’

Rifat Ferdous,¹ Kok W. Chan,² Menno Veldhorst,³ J.C.C. Hwang,² C. H. Yang,²

Gerhard Klimeck,¹ Andrea Morello,² Andrew S. Dzurak,² and Rajib Rahman¹

¹Network for Computational Nanotechnology, Purdue University, West Lafayette, IN 47907, USA

²Centre for Quantum Computation and Communication Technology,
School of Electrical Engineering and Telecommunications,

The University of New South Wales, Sydney, New South Wales 2052, Australia

³QuTech and Kavli Institute of Nanoscience, TU Delft, Lorentzweg 1, 2628CJ Delft, the Netherlands

(Dated: August 3, 2017)

S1. Analytic effective mass model to explain the effect of spin-orbit interaction (SOI) on the g -factors in a silicon (Si) quantum dot (QD)

Here we briefly summarize the effective mass model that qualitatively explains the atomistic tight-binding results in terms of the Rashba and Dresselhaus SOI, shown in the supplementary of ref. [1]. We can write the electron Hamiltonian in a Si QD as,

$$H = \frac{\hbar^2}{2m}\mathbf{k}^2 + V(\mathbf{r}) + H_Z + H_{SO} \quad (\text{Eq. S1})$$

Here, m is the electron effective mass, $V(\mathbf{r})$ is the potential defining the quantum dot. $H_Z = \frac{1}{2}g\mu_B\boldsymbol{\sigma} \cdot \mathbf{B}$ is the Zeeman term, with g the electron g -factor, μ_B the Bohr magneton, and \mathbf{B} the applied magnetic field. $H_{SO} = \beta(\sigma_x k_x - \sigma_y k_y) + \alpha(\sigma_x k_y - \sigma_y k_x)$ is the SOI term, where β (α) is the strength of Dresselhaus (Rashba) interaction, σ_x , σ_y are the Pauli spin matrices, and k_x , k_y are electron canonical momentum along x ([100]) and y ([010]) directions respectively. $\mathbf{k} = -i\nabla - e\frac{\mathbf{A}}{\hbar}$, where \mathbf{A} is the vector potential and $\mathbf{B} = \nabla \times \mathbf{A}$. Now, we treat $H_P = H_Z + H_{SO}$ as a perturbation to $H_0 = \frac{\hbar^2}{2m}\mathbf{k}^2 + V(\mathbf{r})$. The unperturbed Hamiltonian H_0 yields the spin degenerate eigenstates of a Si QD.

We can write the perturbation Hamiltonian separately for each valley as,

$$H_P(v_{\pm}) = \sigma_x \left(\frac{1}{2}g\mu_B B_x + \beta_{\pm}k_x + \alpha_{\pm}k_y \right) + \sigma_y \left(\frac{1}{2}g\mu_B B_y - \beta_{\pm}k_y - \alpha_{\pm}k_x \right) + \sigma_z \left(\frac{1}{2}g\mu_B B_z \right) \quad (\text{Eq. S2})$$

Here, we replaced β, α with $\beta_{\pm}, \alpha_{\pm}$ to denote the two v_+ and v_- valley states [2, 3]. Now, the momentum operator in a magnetic field \mathbf{B} are,

$$k_x = -i\frac{\partial}{\partial x} - e\frac{A_x}{\hbar} \approx -e\frac{A_x}{\hbar} \quad (\text{Eq. S3})$$

$$k_y = -i\frac{\partial}{\partial y} - e\frac{A_y}{\hbar} \approx -e\frac{A_y}{\hbar} \quad (\text{Eq. S4})$$

Since $\langle v_{\pm} | -i\frac{\partial}{\partial x} | v_{\pm} \rangle \approx \langle v_{\pm} | -i\frac{\partial}{\partial y} | v_{\pm} \rangle \approx 0$. For a magnetic field in the x - y plane, we assume, $A_z = 0$, $A_x = zB_y$ and $A_y = -zB_x$, where B_x and B_y are the x and y components of the magnetic field respectively and the z component $B_z = 0$. Then,

$$k_x \approx |e|\frac{z}{\hbar}B_y \quad (\text{Eq. S5})$$

$$k_y \approx -|e|\frac{z}{\hbar}B_x \quad (\text{Eq. S6})$$

and,

$$H_P(v_{\pm}) = \sigma_x \left(\frac{1}{2}g\mu_B B_x + \beta_{\pm}|e|\frac{z}{\hbar}B_y - \alpha_{\pm}|e|\frac{z}{\hbar}B_x \right) + \sigma_y \left(\frac{1}{2}g\mu_B B_y + \beta_{\pm}|e|\frac{z}{\hbar}B_x - \alpha_{\pm}|e|\frac{z}{\hbar}B_y \right) \quad (\text{Eq. S7})$$

It is interesting to note here that, when B_{ext} is along [100], $B_y = 0$ and the Dresselhaus SOI has only off-diagonal contribution (σ_y), and thus has negligible effect to the g -factors. On the other hand, for B_{ext} along [110], $B_x = B_y$ and the Dresselhaus SOI acts as a diagonal term and dominates the g -factor renormalization.

After diagonalizing Eq. S7 we get the spin splitting for different valleys,

$$E_{ZS(\pm)} = 2 \left\{ \left(\frac{1}{2}g_{\perp}\mu_B B_x + \beta_{\pm}|e|\frac{\langle z \rangle}{\hbar}B_y - \alpha_{\pm}|e|\frac{\langle z \rangle}{\hbar}B_x \right)^2 + \left(\frac{1}{2}g_{\perp}\mu_B B_y + \beta_{\pm}|e|\frac{\langle z \rangle}{\hbar}B_x - \alpha_{\pm}|e|\frac{\langle z \rangle}{\hbar}B_y \right)^2 \right\}^{\frac{1}{2}} \quad (\text{Eq. S8})$$

We replaced g here with g_{\perp} , the g -factor perpendicular to the valley axis[4]. When B_{ext} creates an angle ϕ with the [100] crystal orientation in a counter clockwise rotation, $B_x = B_{\text{ext}}\cos\phi$ and $B_y = B_{\text{ext}}\sin\phi$,

$$E_{ZS(\pm)} = g_{\perp}\mu_B B_{\text{ext}} \left\{ 1 + 4 \left(\frac{|e|\langle z \rangle}{g_{\perp}\mu_B \hbar} \right)^2 (\beta_{\pm}^2 + \alpha_{\pm}^2) - 4 \frac{|e|\langle z \rangle}{g_{\perp}\mu_B \hbar} \alpha_{\pm} + 4 \frac{|e|\langle z \rangle}{g_{\perp}\mu_B \hbar} \beta_{\pm} \sin 2\phi - 8 \left(\frac{|e|\langle z \rangle}{g_{\perp}\mu_B \hbar} \right)^2 \beta_{\pm} \alpha_{\pm} \sin 2\phi \right\}^{\frac{1}{2}} \quad (\text{Eq. S9})$$

Now, $1 \gg \left(\frac{|e|\langle z \rangle}{g_{\perp}\mu_B \hbar} \right) \beta_{\pm} > \left(\frac{|e|\langle z \rangle}{g_{\perp}\mu_B \hbar} \right) \alpha_{\pm}$ [3]. So, we can ignore the second order terms. Thus simplifying equation Eq. S9 we get,

$$E_{ZS(\pm)} = g_{\perp}\mu_B B_{\text{ext}} \left\{ 1 - 4 \frac{|e|\langle z \rangle}{g_{\perp}\mu_B \hbar} \alpha_{\pm} + 4 \frac{|e|\langle z \rangle}{g_{\perp}\mu_B \hbar} \beta_{\pm} \sin 2\phi \right\}^{\frac{1}{2}} \quad (\text{Eq. S10})$$

After doing a series expansion and ignoring higher order terms, we can simplify this expression even further,

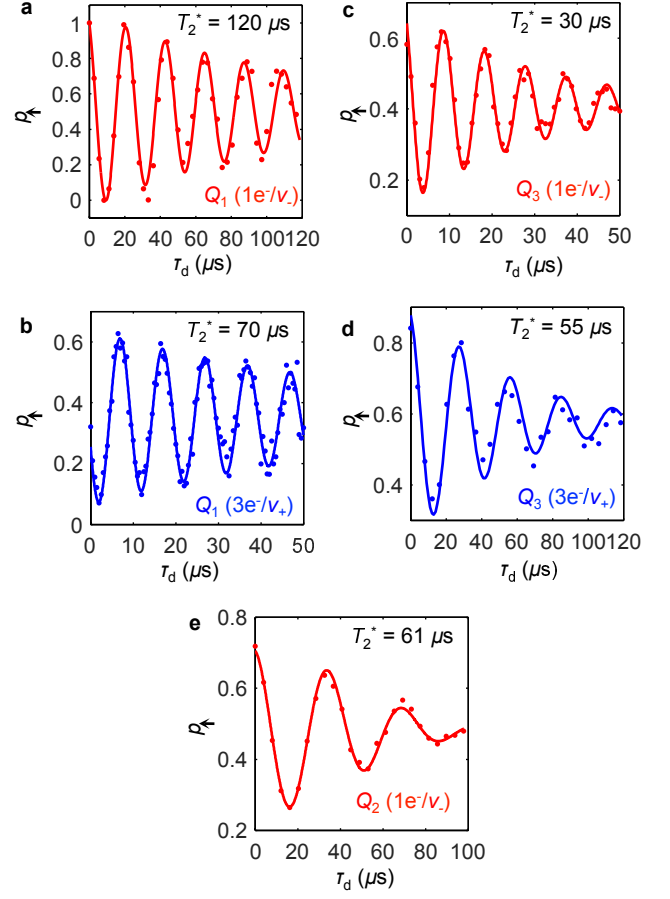
$$E_{ZS(\pm)} = g_{\perp}\mu_B B_{\text{ext}} \left\{ 1 - 2 \frac{|e|\langle z \rangle}{g_{\perp}\mu_B \hbar} \alpha_{\pm} + 2 \frac{|e|\langle z \rangle}{g_{\perp}\mu_B \hbar} \beta_{\pm} \sin 2\phi \right\} \quad (\text{Eq. S11})$$

Writing, $E_{ZS(\pm)} = (g_{\perp} + \delta g_{\pm})\mu_B B_{\text{ext}}$, we get,

$$\delta g_{\pm} \approx 2 \frac{|e|\langle z \rangle}{\mu_B \hbar} (-\alpha_{\pm} + \beta_{\pm} \sin 2\phi) \quad (\text{Eq. S12})$$

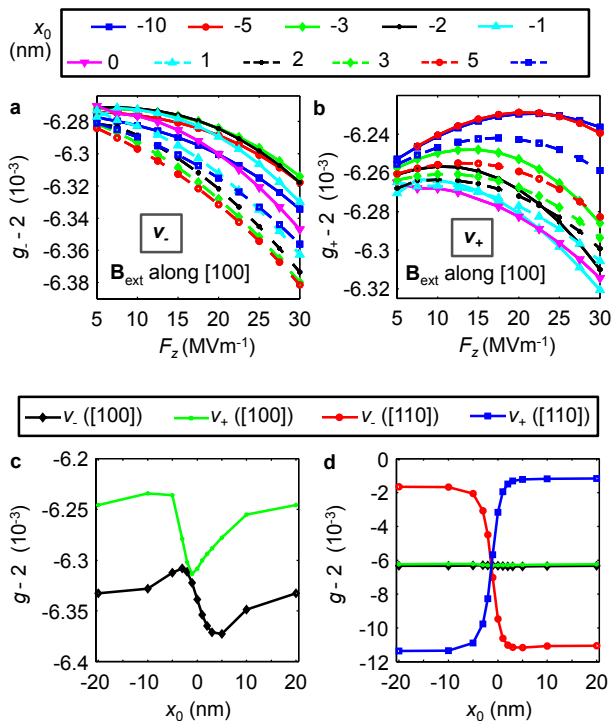
S2. Ramsey experiments

One-electron and three-electron Ramsey oscillations for Q_1 , Q_2 and Q_3 are shown Fig. S1. The dephasing times shown in Fig. 2d of the main text, are extracted from Fig. S1.



Supplementary Fig. S1. Ramsey oscillations for both one-electron (v_-) and three-electron (v_+) qubits in Q_1 and Q_3 , and one-electron (v_-) qubit for Q_2 in sample A

S3. g -factors in a Si QD with the external magnetic field along the [100] crystal orientation



Supplementary Fig. S2. Change in g_- (a) and g_+ (b) as a function of F_z for different distances from the interface step to the dot center, x_0 , with B_{ext} along [100]. (d) g_{\pm} as a function of x_0 for B_{ext} along [100], for $F_z = 28.5 \text{ MVm}^{-1}$. (c) Comparison in g_{\pm} as a function of x_0 between B_{ext} along [100] and [110], for $F_z = 28.5 \text{ MVm}^{-1}$.

In Fig. S2 we show the changes in the g -factors with interface step position and electric field for B_{ext} along [100]. Figs. S2a and S2b show g_- and g_+ respectively as a function of F_z for different values of x_0 . It can be seen that the range of change with both F_z and x_0 is much smaller compared to that in Figs. 1c and 1d of main text, when B_{ext} is along [110]. In Fig. S2d we compare the change in g -factors between [100] and [110] with respect to x_0 for $F_z = 28.5 \text{ MVm}^{-1}$. Though there are variations in g_- and g_+ due to the change in the location of the dot from an interface step when B_{ext} is along [100], as shown by Fig. S2c, these variations are negligible compared to that when B_{ext} is along [110].

- [1] R. Ferdous, E. Kawakami, P. Scarlino, M. P. Nowak, D. R. Ward, D. E. Savage, M. G. Lagally, S. N. Coppersmith, M. Friesen, M. A. Eriksson, L. M. K. Vandersypen, and R. Rahman, (2017), arXiv:1702.06210.
- [2] M. Veldhorst, R. Ruskov, C. H. Yang, J. C. C. Hwang, F. E. Hudson, M. E. Flatté, C. Tahan,

- K. M. Itoh, A. Morello, and A. S. Dzurak, Phys. Rev. B **92**, 201401 (2015).
- [3] M. O. Nestoklon, E. L. Ivchenko, J.-M. Jancu, and P. Voisin, Phys. Rev. B **77**, 155328 (2008).
- [4] L. M. Roth, Phys. Rev. **118**, 1534 (1960).